

degrees in the case of the X2 flare. For the other 18 M-class flares, about half showed an increase, the other half a decrease, but in all cases the changes were on the order of the noise level. A study of five X-class flares (Wang, *et al.*, 1994) showed dramatic increases in shear during the flare, ranging in values from 5-40 degrees in the area of the neutral line.

It is not only this discrepancy in observed changes that is problematical. There are the problems associated with determining the actual cause of the changes and whether they are indeed directly related to the flare itself. For example, there are instrumental effects which can produce changes in the measured linear polarization which translate into changes in the magnetic field azimuth and transverse field strength. These instrumental effects include the so-called circular cross-talk where circularly polarized signals are mixed into the linear signal, instrumental linear polarization, and field-of-view errors introduced by the birefringent electro-optical modulators used in some polarimeters. Then there are changes induced by variable “seeing” during the observations. The Sun itself can be the culprit. Photospheric oscillations might affect the value of magnetic shear, for, although the azimuth measurements are not altered by doppler shifts in the line profile, the potential azimuth can be affected since it is based on measurements of the line-of-sight field that are influenced by doppler shifts. And the ongoing evolution of the active region field itself can produce changes that may be mistakenly identified with the flare event. Such evolutionary changes can moreover alter the line-of-sight field used to compute the potential field and thus alter the potential azimuth orientation which is used in the calculation of the shear angle.

Observations with the MSFC vector magnetograph of the active region AR6659 on June 10, 1991, produced a set of data that provided us the opportunity to carefully test the association of changes in the magnetic field with flare events. The salient features of this data set that make it especially suited to this research are: (1) it covered almost the entire observing day from 12:07 UT to 21:19 UT; (2) 70 vector magnetograms were obtained in this time period with long intervals where the data were obtained with a 4-6 minute cadence; (3) the data were carefully calibrated for circular cross-talk and instrumental linear polarization; (4) the observing conditions were good throughout the day; (5) the observations spanned 2 M-class flares.

In this paper we present the results of our analysis of these data. We focus our analysis on just the azimuth of the field since it is the only field component that is directly derived from the observed linear polarization data and is free from effects of calibration techniques and doppler shifts in the line profile. Our analysis shows (1) the rms variation of the azimuth of the field has a peak distribution of 2° over the field of view of this active region for an interval of 6 hours (12:07 - 18:06 UT), and (2) there is no really significant association of changes in the azimuth with the two flares. In Section 2 we discuss the observational data and our method of data reduction, in Section 3 we present our analysis to identify changes in the azimuth, we discuss our findings in Section 4, and we present a summary in the last section.

2. Observations and Data Reduction Techniques

The active region NOAA AR 6659 was extremely flare productive, with 6 flares of classification greater than X10 occurring during its disk passage. On June 10 the region was

located at N31W06 and two M-class flares took place, a 1N/M6 at 13:53 UT (with flare maximum at 13:56), and a SN/M3 at 16:53 UT (maximum at 16:54). MSFC observations were taken from 12:07 to 18:06 UT in the morning with 57 vector magnetograms obtained; the telescope was turned for the afternoon observing starting at 19:08 UT and ending at 21:19 UT with 13 magnetograms taken. The longest time “gap” in the morning observations was 26 minutes, but in the interval 13:13 - 17:34 that spanned the two flares, data were taken with cadences of 4 - 6 minutes, and the longest gaps were two 11-minute intervals that were after the last flare.

2.1 DATA REDUCTION OF MSFC VECTOR MAGNETOGRAMS

The MSFC vector magnetograph is a filter-based instrument employing a tunable 0.125 Å Lyot filter and an electro-optical modulator to obtain integrated Stokes intensities in the Fe I 5250.22 Å absorption line (Hagyard *et al.*, 1982). The data reduction process starts with an evaluation of the circular cross-talk derived from special cross-talk calibrations that were performed at 12:00, 13:00, 18:00, 19:00, and 20:00 UT. These data were used to interpolate for the cross-talk values used in the calibration of the magnetograms taken at other times. (There was very little change in the cross-talk between 13:00 and 18:00 UT: it ranged from -2.22% to -1.38% for the U-Stokes intensity and from 2.15% to 3.07% for the Q parameter.) To determine the instrumental polarization, each vector magnetogram is analyzed for a linear polarization bias using distribution plots of number of pixels vs. Q/I and U/I. The intensities (I) for the Stokes U, Q, and V are all normalized using a set of data taken away from the active region with the telescope defocused.

Following these corrections for cross-talk and instrumental polarization, the resulting polarized intensities are converted to magnetic field values using the procedure outlined in Hagyard and Kineke (1995). All of the magnetograms were calibrated to the same maximum field strength of 2500 G. While this value is lower than field strengths measured by other instruments for this active region, its choice will not affect the analysis of the azimuth since its value is independent of the chosen maximum field strength.

2.2 REGISTRATION TECHNIQUE

To perform the subsequent analyses, the vector magnetograms all had to be co-registered. We selected 1 magnetogram as the template and registered all the others with it. In the data reduction process, for a single magnetogram, there are 6 measured intensities obtained in the following order: $I_V \pm V$, $I_Q \pm Q$, and $I_U \pm U$; these yield V/I_V , Q/I_Q , and U/I_U . To register these 3, the intensities I_V , I_U are registered with I_Q using sub-pixel interpolation; then the normalized Stokes intensities V/I_V , U/I_U are registered with Q/I_Q with the same interpolation. In registering the different magnetograms with the template magnetogram, the process is started by registering the intensity I_Q with that of the template I_Q^T ; then the V and U components of the magnetogram are registered with I_Q .

In applying this sub-pixel registration to the complete set of data, we found the registration of the afternoon data difficult for 3 reasons: (1) there was a 62-minute gap in time between the morning and afternoon observations, (2) the telescope has to be turned over for the afternoon observing and there were no photometric calibration data taken in the afternoon observing period, so we had to use the morning calibration data to normalize

the intensities, and (3) the template magnetogram was taken in the early morning. Because of the ensuing difficulty in registering the afternoon data, we only used the morning data in this study.

The data reduction process described above produced 57 vector magnetograms that were all registered to sub-pixel accuracy, corrected for cross-talk and instrumental polarization, and calibrated to the same maximum field strength. To deal with the 180-degree ambiguity in the azimuth, we compared the azimuth of each magnetogram with the azimuth of the template at every pixel and chose the azimuth closest to that of the template.

3. Analysis for Flare-Associated Azimuth Changes

3.1 THE MAGNETIC FIELD MORPHOLOGY

Figure 1 shows the vector magnetic field of AR6659 obtained from the template magnetogram taken at 14:32 UT. A notable feature of this region is the predominance of negative flux of the main spots, surrounded by positive flux. There are two main magnetic neutral lines, bordering, respectively, the eastern and western parts of this negative flux. In Figure 1c we see the particular signature of sheared magnetic fields along the northeastern and southwestern sections of this neutral line: the direction of the transverse (to the line-of-sight) field indicated by the line segments lies along, rather than across, the neutral line. The transverse field of this region was also particularly strong, especially in the vicinity of the northeastern neutral line. The magnetic field in this latter area therefore was highly stressed and contained sufficient free energy to fuel all the large X-class flares that this region produced, not surprisingly along this northeastern neutral line. However, numerous other flares took place in this region, including 25 M-class events, and these were seen to erupt along other sections of the neutral line.

3.2 LOCATIONS OF THE TWO FLARES

The H-alpha telescope that is coaligned with the MSFC vector magnetograph gives us digitized video images of the region under study with the magnetograph. Normally three H-alpha images are digitized during the acquisition of a single vector magnetogram; during higher levels of activity, we can video-tape the H-alpha images for more continuous coverage. We have developed an analysis program that scales the digitized H-alpha image to the vector magnetogram field of view and then registers the re-scaled H-alpha image to a magnetogram. In our analysis of the two M-class flares of June 10, we registered the H-alpha images to the template magnetogram, so they would be registered to all 57 of the magnetograms we included in this study. In Figures 2 and 3 we show the registration of the H-alpha and template magnetic field for the first and second flares, respectively. We used the images of Figures 2b and 3b to define the pixels in the magnetograms that are in the areas of the primary flare emission.

3.3 MAGNETOGRAMS BEFORE AND DURING THE FLARES

A qualitative method to look for flare-related azimuth changes is to compare directly the vector magnetic field before and after the start of a flare. We show this method in Figure 4a and 4b for the first and second flares, respectively. In these figures we superimpose

the azimuth orientations of the magnetograms taken after the start of the flare with those of magnetograms taken just before the flares. This direct comparison does not indicate any significant changes in the azimuth in the areas of the H-alpha emission identified in Figures 2b and 3b in light of the fact that similar or larger changes are seen in areas away from the flares.

3.4 QUANTITATIVE ANALYSIS FOR AZIMUTH CHANGES

We used the following quantitative method to look for changes in the azimuth. At each pixel in the field of view of Figure 1 we calculated the rms fluctuation, in time, of the azimuths for the 57 magnetograms spanning the time period 12:07 - 18:06 UT. Any change in the azimuth as a function of time is expected to produce a discernible increase in the rms value, provided the changed state lasts for a significant fraction of the observing interval. In Figure 5 we show a histogram of the rms fluctuations, $\delta\phi$, for all pixels with transverse field strength ≥ 200 G. (A similar histogram is obtained for a cutoff value of 50 G with the primary difference being higher-valued $\delta\phi$'s in the tail of the distribution.) In the plot the abscissa is the number of bins of the azimuth with the units represented by one such bin of 1° . The ordinates are the number of pixels (out of the 61×61 pixels examined) that possess the value represented by the abscissa. For example, there are 400 points whose azimuths changed on the order of $\pm 1^\circ$ from their mean value over a period of 6 hours. Note that the most probable value of rms azimuth fluctuation is 2° which then fixes the mean level of uncertainty in azimuth measurement for the field of view under consideration.

This histogram indicates there are pixels with $\delta\phi$ in the range of 20-40 degrees; these would be notable changes if related to the flares. To focus on significant changes in the vicinity of the two flares, a map of $\delta\phi$ was generated to see its spatial distribution; this map is shown in Figure 6a. In Figure 6b we have reproduced the image of Figure 1c and superposed on it the flare kernels (heavy dashed curves) and areas where there are pixels with $\delta\phi \geq 10^\circ$ and $B_T \geq 200$ G (heavy solid curves). (We used the transverse field strength values from the template magnetogram for the criterion of 200 G.) From this figure we see that most of the area of the active region has no large fluctuations, in agreement with the histogram. However, there are several areas of large $\delta\phi$ near the flares which require more detailed analysis to determine the source of the variations and any relationship to the flares.

3.5 AZIMUTH VARIATIONS WITH TIME

In this analysis we looked at the temporal change in the measured azimuth at pixels in the flare region. These pixels were selected using Figures 2b and 3b which identified pixels covered by the initial flare emission; the coordinates of these pixels in the magnetograms were then identified. For each one of these selected pixels we plotted its azimuth ϕ versus time for the 57 magnetograms covering the interval 12:07 - 18:06 UT. We then looked for "significant" changes in the azimuth near the times of the two flares, where a significant change is one that is clearly greater than the point to point variations seen at other times in the sequence for that particular pixel.

3.5.1 The Flare at 13:53 UT

This flare had two main areas of emission at flare maximum, kernel #1 in the negative polarity along the eastern part of that section of the western neutral line (to the left in Figure 2b) and kernel #2 in the positive polarity to the west of kernel #1.

Kernel #1 covered 21 pixels of the template magnetogram, and the ϕ vs. time plots for these 21 pixels showed no significant changes near 14:00 UT. Figure 7a shows these plots for the 6 pixels in the area of most intense H-alpha emission, and they are representative of all pixels in this kernel. The transverse field strength at these 6 pixels was greater than 1000 G and the $\delta\phi$ ranged from 3.0° to 5.7° . For all the pixels we found $2.0^\circ \leq \delta\phi \leq 7.2^\circ$; for the 3 pixels with the largest $\delta\phi$, shown in Figure 7b, the largest changes in azimuth are seen to occur well after 14:00 UT. Note the evolutionary change in ϕ for some of these pixels; for example, the top curve of Figure 7a indicates the azimuth gradually increased by ~ 20 degrees over the 6-hour interval; the rms variation $\delta\phi$ at this pixel was 5.6° .

The second kernel covered 29 pixels in the magnetograms. Of these, 21 were outside the heavy solid contours of Figure 6b that delineate areas where the rms variations in azimuth were greater than 10° and $B_T \geq 200$ G. For these 21 pixels, there were 17 with $2^\circ \leq \delta\phi \leq 6^\circ$; the remaining 4 had rms variations of 9, 14, 42, and 47 degrees. For the 17 pixels with low $\delta\phi$, we found no changes in azimuth near 14:00 UT that were significantly larger than changes at other times. In the case of the pixel with $\delta\phi = 9^\circ$, the large variations in azimuth that contributed to this value occurred well after 14:00 UT. For the other 3, the large variations in azimuth all took place at times when the transverse field strength fell well below 250 G. This correlation is shown in Figures 8a,b where we have plotted the time-variations of the azimuth and transverse field strength for the pixel with $\delta\phi = 47^\circ$.

From our analysis of the 8 pixels inside the contours of Figure 6b we found no changes greater than others near 14:00 UT for pixels with transverse fields ≥ 250 G in the time period of 14:00. But again we determined that when the transverse field strength dropped below 250 G at any particular time, then there were large variations in ϕ at that time. We show this result in Figures 8c,d where we have plotted the variations of the azimuth and the transverse field strength for the pixel with the largest rms variation in azimuth of these 8 pixels ($\delta\phi = 28^\circ$).

We should not be surprised at the conclusion that $\delta\phi \sim 1/B_T$, and in Figure 9 this relation is demonstrated in plotting the rms variation at each pixel versus the average transverse field strength at that pixel. Our analysis for areas of large $\delta\phi$ using Figure 6b did not account for temporal variations in field strength which led to B_T values dropping below 200 G over short time intervals even though the average field strength was above that value.

3.5.2 The Flare at 16:53 UT

This flare also had two initial areas of emission, the more southerly kernel (area #1) in the negative polarity along the eastern neutral line, and the 2 kernels to the north in the positive polarity (area #2). There were 22 pixels of the magnetogram in the southern kernel. All of these had $\delta\phi \leq 3.5^\circ$ with the exception of 3 pixels ($\delta\phi = 3.9^\circ, 5.7^\circ, 11.3^\circ$). But we observed significant (i.e., greater than average) variations in ϕ near the time of the flare for about one-half of the 22 pixels. On the other hand we also observed similar and in some cases larger variations away from the emission area. In Figure 10a we have

plotted the azimuth variations for 4 pixels in the kernel; they all exhibit an increase in azimuth starting just before 17:00 UT that is larger than the rms variations at other times. The changes in azimuth during the interval 16:43-17:17 UT ranged from 7 to 9 degrees, small changes but larger than the rms variations that were $\leq 3.2^\circ$. The time-variation of azimuth for 3 pixels outside the initial H-alpha emission is shown in Figure 10b. For these 3 pixels the change in azimuth for the same time interval was 8, 8, and 9 degrees; their rms variations were 8.5° for the lowest curve and 2.2° for both upper curves. The pixel of the lowest curve was located to the east of the kernel in the positive-polarity flux east of the neutral line; the other two pixels were to the west of the kernel in the negative polarity. It is interesting that all the pixels shown in Figures 10a and 10b have similar profiles for the change in azimuth near 17:00 UT; other pixels not shown in these figures have profiles that resemble these but their changes in azimuth are smaller.

We looked at the time profiles for the line-of-sight and transverse components of the magnetic field (B_L and B_T , respectively) and the measured intensity I_Q at the pixels that showed the jump in azimuth near 17:00 UT. We saw nothing in the B_L time profile that correlated with the azimuth changes. However, in each case there were abrupt changes in I_Q and B_T that were coincident in time with the increase in azimuth. In the case of I_Q the changes were all positive and small, on the order of 2-3% ($I_Q \sim 660$ counts), and they were comparable to other abrupt changes in intensity over the time of the observations (so it seems unlikely that this increase in intensity was caused by heating of the photosphere due to the flare). The transverse component dropped in every case, on the order of 165 G, and then recovered with a net drop of about 50 G. These initial drops in the transverse component were larger than other changes in B_T in the time profile for most pixels. There did not seem to be any quantitative correlation between the jumps in intensity and field, i.e., larger changes in B_T were seen for pixels with smaller changes in intensity. Also, whereas both B_T and I_Q increase from 16.8-16.9 UT and then relax towards their initial values, the azimuth continues to increase beyond this interval well past 17.0 UT. We cannot rule out a relation of these changes with the flare that started at 16.9 UT. But in the case of the azimuth, which is our main focus, the changes were all small, $\leq 9^\circ$ for pixels in the flare kernel, and larger changes were seen away from the flare. These results, then, are not unambiguous, and we fall back on that old refrain, "more cases need to be studied".

The initial flare emission in area #2 covered 27 pixels of the magnetogram, some of which were in the areas of large values of $\delta\phi$ (the largest was 25°). But our conclusions here were identical to those for kernel #2 of the earlier flare: we found no significant changes in the azimuth near 17:00 UT for pixels with $B_T \geq 250$ G near that time. In the case of the pixels with large rms azimuth variations, they all exhibited erratic behavior in the azimuth's time profile beginning at the time when the field strength falls below ~ 250 G. However, many of these profiles in area #2 do indicate that the azimuth was undergoing evolutionary changes, and we discuss this in the following section.

3.6 EVOLUTIONARY CHANGES OF THE AZIMUTH

A number of pixels analyzed in this study exhibited an evolutionary change in the azimuth, i.e., the azimuth changed gradually over the 6-hour observing interval with a resulting increase or decrease of 10-20 degrees. To study this evolution, we analyzed all the pixels in the flare emission of both flares by plotting filtered time profiles of the azimuth to depress

the short-term fluctuations and noted pixels with larger than 10-degree changes and $B_T \geq 250$ G. We discuss our results for the four areas of emission in the two flares.

In the eastern kernel of the first flare, 13 of 21 pixels exhibited $11^\circ \leq \Delta\phi \leq 22^\circ$; the time profile for a typical pixel is shown in Figure 11a. In the western kernel of this flare, of the 29 pixels studied, 18 had $11^\circ \leq \Delta\phi \leq 40^\circ$; 2 of these cases are shown in Figure 11b. To summarize our findings for the first flare: most changes in the azimuth ϕ show a similar trend, i.e., to make ϕ more aligned in the east-west direction; most of the changes result in a more non-potential orientation; and there are 10 pixels where $\Delta\phi \leq 5^\circ$.

The analysis for the southern kernel of the second flare produced the following results: out of the 22 pixels, 10 showed $\Delta\phi \leq 5^\circ$, 10 showed $6^\circ \leq \Delta\phi \leq 10^\circ$, and 2 showed $\Delta\phi \geq 10^\circ$. In Figure 11c filtered time profiles for 2 pixels are shown, one with no change, the other with a large change. In the upper or northern half of this kernel, the changes tended to make the azimuth aligned in a more vertical or north-south direction, and perhaps more sheared. In the lower half, the changes made the azimuth somewhat less vertical.

In our analysis for the northern kernel, area #2, we chose only those pixels out of the total of 27 for which $B_T \geq 250$ G for a sufficiently long interval of time to exhibit any evolution. We found: 8 pixels with $\Delta\phi \leq 10^\circ$, 12 pixels with $10^\circ < \Delta\phi \leq 20^\circ$, and 1 pixel with $\Delta\phi > 20^\circ$. The majority of these changes tended to align the azimuth in a more east-west (horizontal) direction, but we could not determine how this alignment affected the non-potentiality of the field because of the convoluted nature of the magnetic neutral line in this area. Figure 11d shows filtered time profiles for 5 pixels.

We continued this analysis for five areas away from both flares. In four of these areas we found $\Delta\phi \leq 10^\circ$. In Figure 12a we show the filtered time profile for 2 pixels in one of these areas, located north of the maximum negative polarity in Figure 1a and about half-way between the two flares. In the fifth area, just to the south of the southern negative umbra, we found $7^\circ \leq \Delta\phi \leq 19^\circ$; azimuth plots for two of these pixels are shown in Figure 12b. In this area the azimuths were all rotating clockwise from an original \sim north-south (vertical) orientation.

The results of this analysis indicate that these evolutionary changes were taking place in different areas of the active region and were not limited to just the flaring areas. We conclude therefore that the changes observed in the azimuths in the flare kernels were not caused by the flares but they may have contributed to the buildup of free energy in the field. However, the flare process did not alter the evolutionary process.

4. Discussion

Ever since the magnetic field was deemed the most probable source of energy for solar flares, there has been the expectation, based on the virial theorem, that coronal changes in this free energy must be visible at the photospheric boundary (Low,1985). In certain cases, cited in the introduction, this expectation has been realized. However, in this study, our search for changes in the azimuth of the photospheric field produced a negative result for the first (and more energetic) flare, and, at best, a weakly positive result for the second event. Perhaps this underscores that the photospheric field may be non-force-free and

would then respond only to changes forced by the dynamics of the photosphere and the convection zone beneath it. A coronal change would be felt only by that part of the field which is force-free, as an electrodynamic response, rather than a mechanical response. We therefore speculate that the expected changes in the magnetic field azimuth could have occurred in a layer of the atmosphere above the observed layer, where the field possessed a force-free character.

This study produced other findings. (1) We found similar time profiles of the azimuth for neighboring pixels, but this correspondence did not hold for well-separated pixels; this result is illustrated in Figure 13. We have not analyzed this phenomenon to determine the scale over which the correlation holds, but we see similar correspondences for the line-of-sight and transverse components of the field. (2) Analysis of Figure 9 and similar data indicates that the threshold value for our measurement of the transverse field is ~ 50 G. (3) There does not appear to be any increase in the intensity I_Q as a result of the flare emission, compared to changes observed at other time intervals.

5. Summary

A careful analysis of a time sequence of vector magnetograms of AR 6659 observed on 1991 June 10 with the MSFC vector magnetograph revealed no significant changes in the vector magnetic field azimuths associated with the M6 flare at 13:53 UT and only very minor changes for the M3 flare at 16:53 UT that may or may not be related to the flare itself.

Acknowledgements

This work was initiated when P. Venkatakrishnan was a National Research Council Senior Associate at the NASA/Marshall Space Flight Center. This work is supported by the Solar Physics Office of the Space Physics Division at NASA Headquarters.

References

- Ambastha, A., Hagyard, M. J., and West, E. A.: 1993, *Solar Phys.* **148**, 277.
- Chen, J., Wang, H., Zirin, H., and Ai, G.: 1994, *Solar Phys.* **154**, 261.
- Gary, G. A., Moore, R. L., Hagyard, M. J., and Haisch, B. M.: 1987, *Astrophys. J.* **314**, 786.
- Hagyard, M. J., Cumings, N. P., West, E. A., and Smith, J. E.: 1982, *Solar Phys.* **80**, 31.
- Hagyard, M. J., Smith, J. B., Jr., Teuber, D., and West, E. A.: 1984, *Solar Phys.* **91**, 115.
- Hagyard, M. J., and Kineke, J. I.: 1995, *Solar Phys.* **158**, 11.

Low, B. C.: 1985, in M. J. Hagyard (ed.), *Measurements of Solar Vector Magnetic Fields*, NASA Conference Publication 2374, p. 49.

Wang, H.: 1992, *Solar Phys.* **140**, 85.

Wang, H., Ewell, Jr., M. W., Zirin, H., and Ai, G.: 1994, *Astrophys. J.* **424**, 436.

Figure Captions

Figure 1. Vector magnetogram of AR 6659 obtained at 14:32 UT on 1991 June 10. North is at the top of the map; east is to the left. The field of view is 2.5 arc min^2 for this and subsequent images. (a) Line-of-sight component with solid (dashed) contours representing positive (negative) flux; contour levels are 10, 100, 500, 1000, 1500, 2000, and 2500 G. (b) Transverse component; contour levels range from 200 G to 1400 G in steps of 200 G. (c) Line-of-sight component with superimposed line segments representing the orientation and magnitude of the transverse component; line segments are scaled from 125 G to 500 G. (d) The intensity I_Q showing the main umbrae of the active region; contour levels range from 400 to 1000 in steps of 100 on a relative scale.

Figure 2. The M6 flare in H-alpha at 13:53 UT. (a) H-alpha image at 13:53 UT with line-of-sight magnetogram at 14:32 UT superimposed (Fig. 1a). (b) Sub-section of the H-alpha image with transverse field (Fig. 1c) superimposed; this shows the azimuth orientations at the start of the flare.

Figure 3. The M3 flare in H-alpha at 16:53 UT. Panels are same as in Fig. 2.

Figure 4. Comparison of the azimuths of the vector magnetic fields before and after the start of the two M-class flares. (a) The M6 flare at 13:53 UT. The azimuths in the area of the flare at 14:09 UT are superimposed on those of the same area at 13:46 UT. (b) The M3 flare at 16:53 UT. The azimuths in the area of the flare at 17:04 UT are superimposed on those of the same area at 16:43 UT.

Figure 5. Histogram of the rms variations of the azimuth for 57 vector magnetograms spanning the period 12:07-18:06 UT. Points with $B_T < 200 \text{ G}$ were excluded; the binning was in 1° increments.

Figure 6. Spatial distribution of the rms variations of the azimuth over the field of view of 2.5 arc min^2 . (a) Contours of rms variations $\delta\phi$. Contour levels are 5, 10, 20, 30, 40, 50, and 65 degrees. The heavy contour outlines the transverse field contour of 200 G of Fig. 1b. (b) The vector magnetogram of Fig. 1c with the areas of panel (a) where the transverse field is $\geq 200 \text{ G}$ and $\delta\phi \geq 10^\circ$ outlined by the heavy solid curves and the flare kernels outlined by the heavy dashed curves.

Figure 7. Variation of azimuth with time for pixels in the eastern kernel of the M6 flare at 13:53 UT. (a) The 6 pixels in the area of most intense H-alpha emission. (b) The pixels with the 3 largest values of $\delta\phi$.

Figure 8. Large variations of azimuth near the time of the M6 flare at 13:53 UT in the western kernel. (a), (b) Variations of the azimuth and transverse field strength for the pixel with the largest $\delta\phi$ in this flare kernel (47°). The large azimuth changes occur when the transverse field falls below 200 G. (c), (d) Similar plots for the pixel with the largest rms variation within the area where $\delta\phi \geq 10^\circ$ and $B_T \geq 200 \text{ G}$. Again, the erratic temporal behavior of the azimuth is a result of the weak transverse field.

Figure 9. The relation between the rms variation of the azimuth $\delta\phi$ and the strength of the transverse field. This shows that the very large values of $\delta\phi$ seen in the histogram of

Fig. 5 were for pixels with very weak transverse fields. It also indicates a threshold of ~ 50 G in our measurement of B_T .

Figure 10. Variation of azimuth with time for pixels in the southern kernel of the M3 flare at 16:53 UT. (a) Azimuth variations for 4 of the pixels that exhibited the anomalous jump in azimuth that began at 16:43 UT. (b) Azimuth variations for 3 pixels outside the flare kernel that also showed this change.

Figure 11. Evolutionary changes of the azimuth over the observing interval 12:07-18:06 UT. Smoothed plots of azimuth vs. time are shown for representative pixels in the emission areas of the two flares. (a) Eastern kernel of the M6 flare at 13:53 UT. (b) Western kernel of this flare. (c) Southern kernel of the M3 flare at 16:53 UT. (d) Northern kernels of this flare.

Figure 12. Evolutionary changes of the azimuth for non-flare areas. (a) Smoothed plots of azimuth vs. time for 2 pixels that showed no evolution. (b) Smoothed plots for 2 pixels that did show gradual changes in azimuth over the 6-hour period of observations.

Figure 13. The correspondence of time profiles for neighboring pixels. (a) Azimuth vs. time for two contiguous pixels. (b) A similar plot for two widely separated pixels.

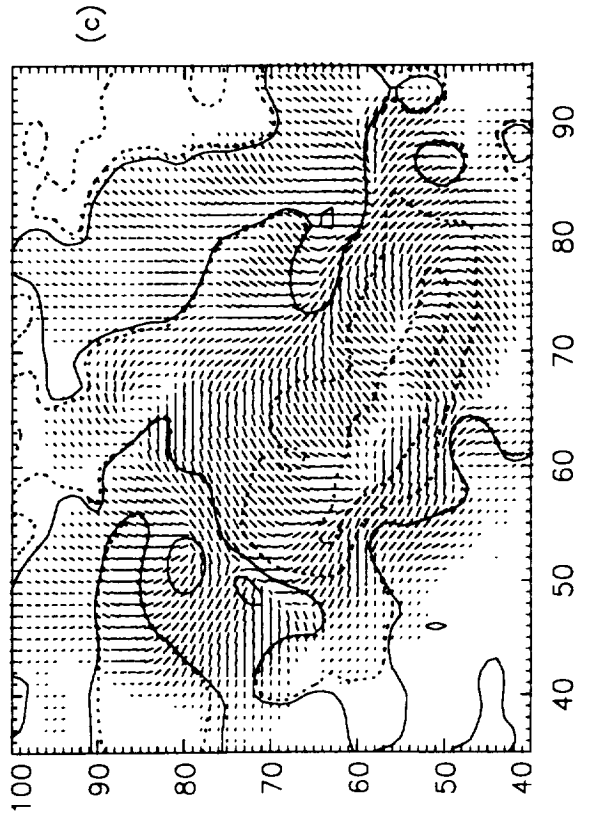
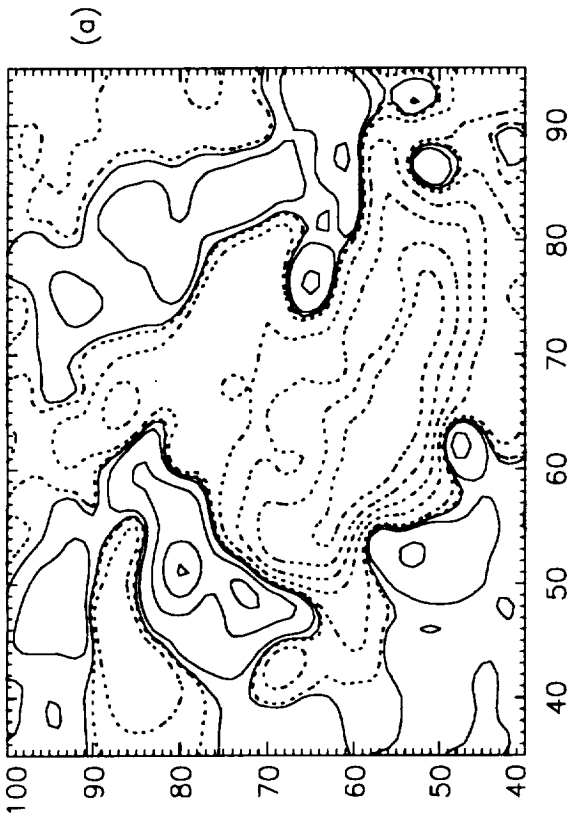
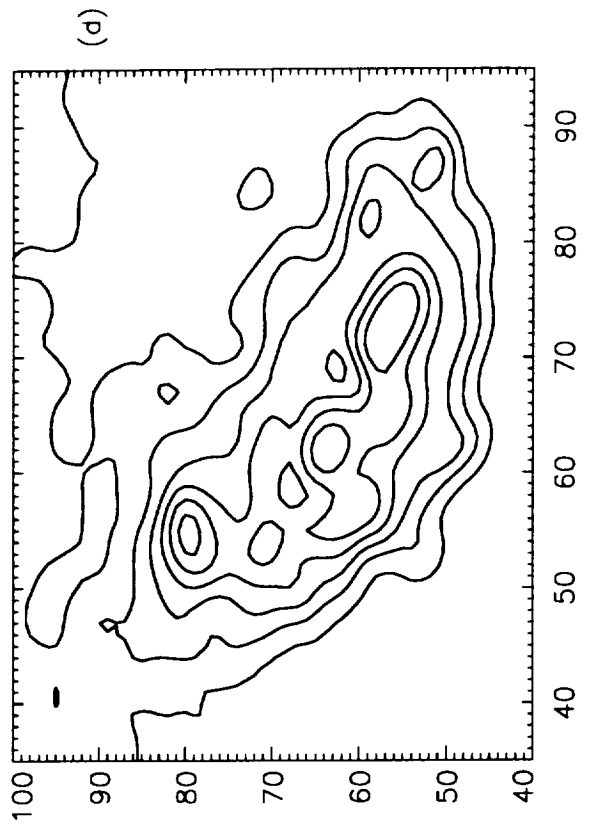
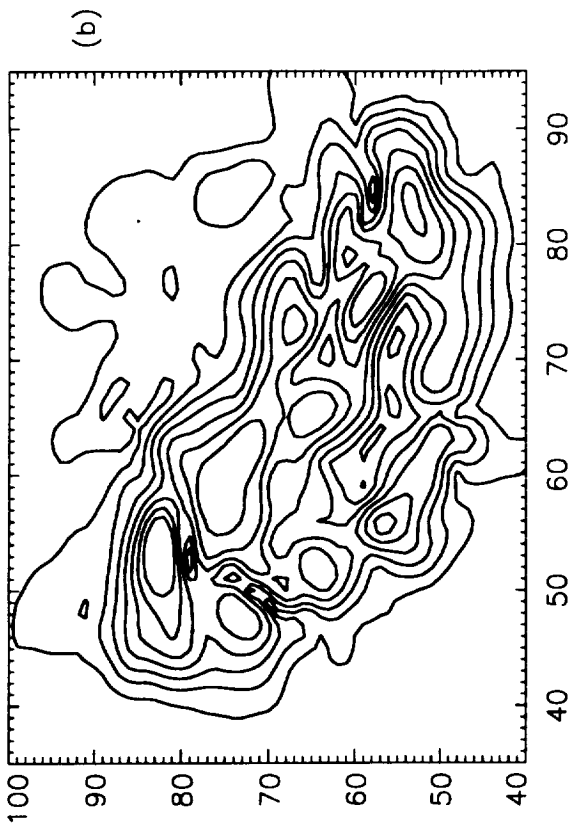
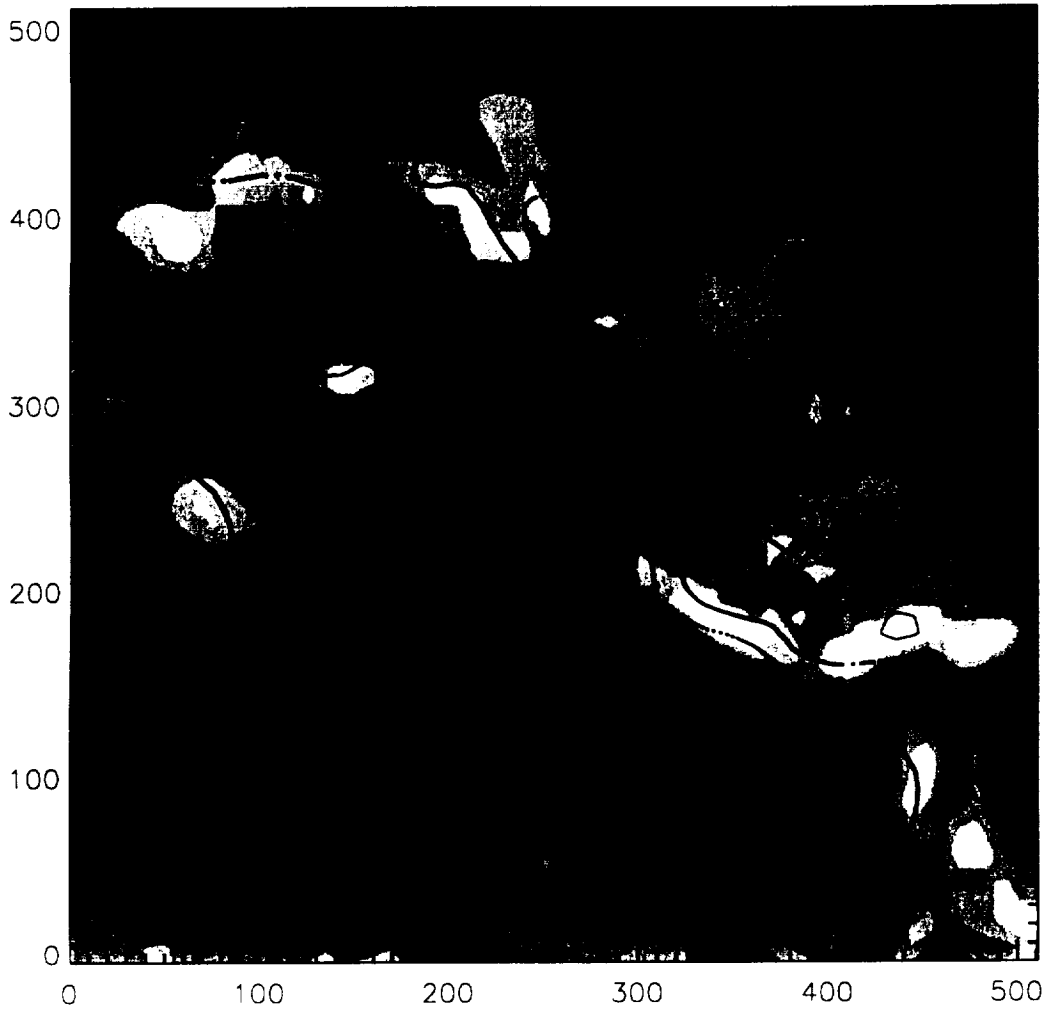
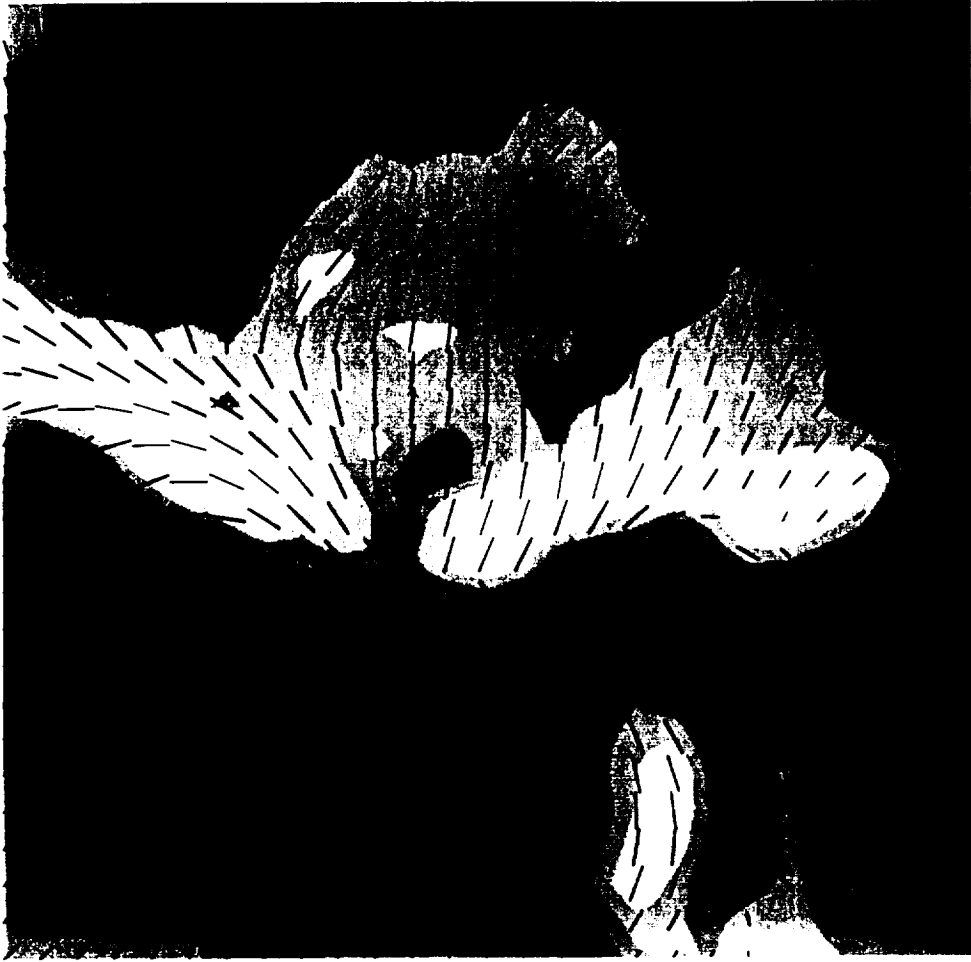


Fig. 1



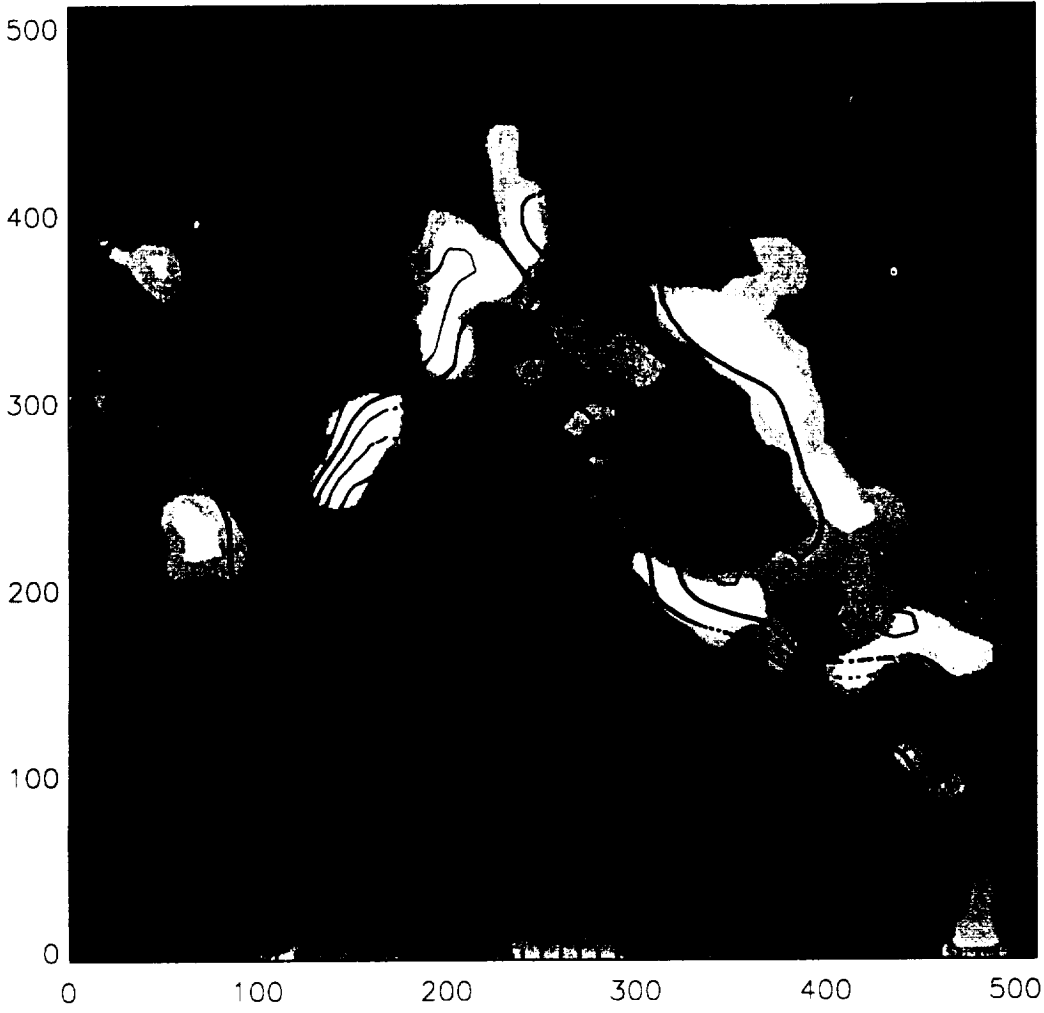
(a)

Fig. 2a



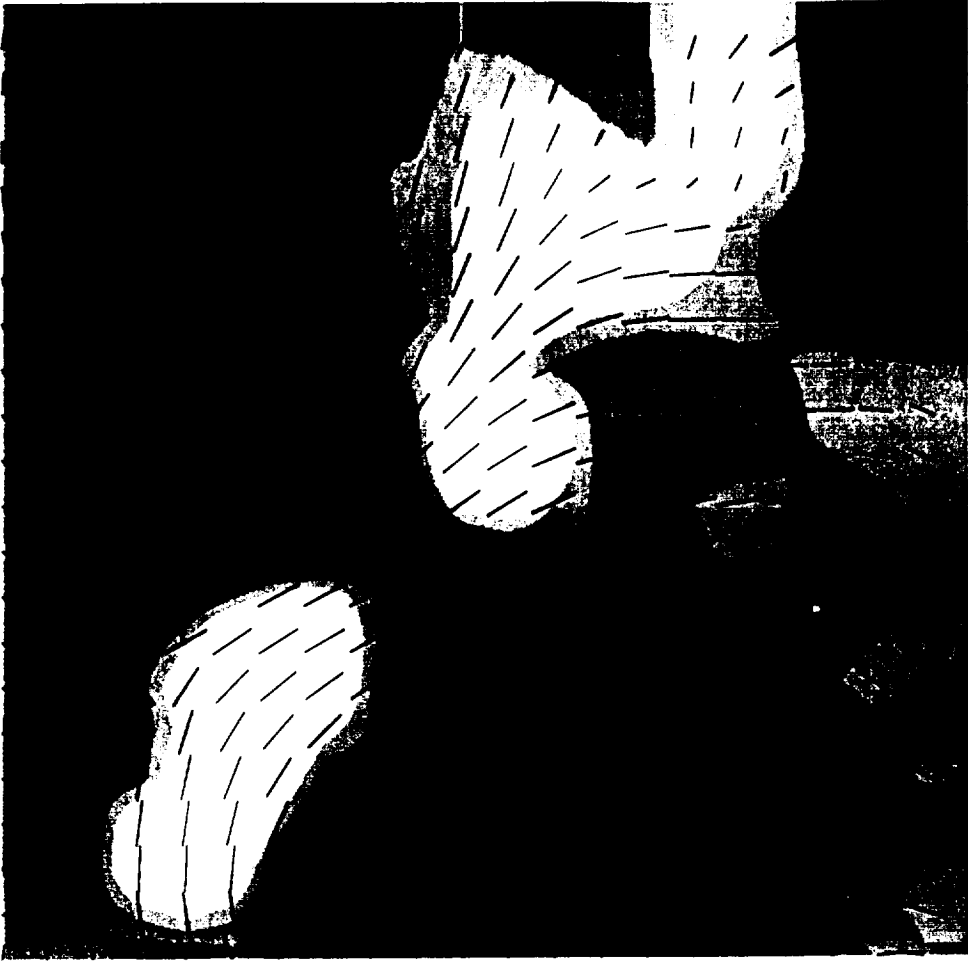
(b)

Fig. 3a

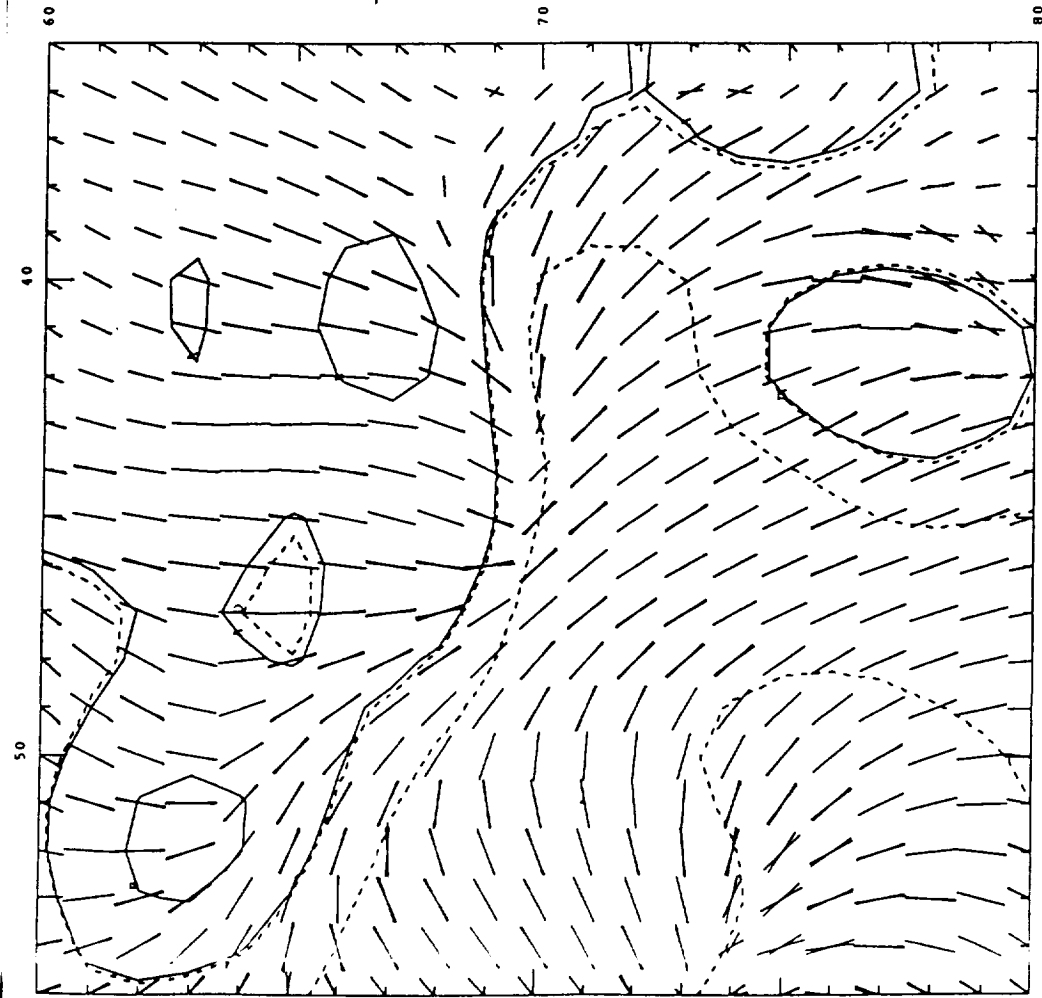


(a)

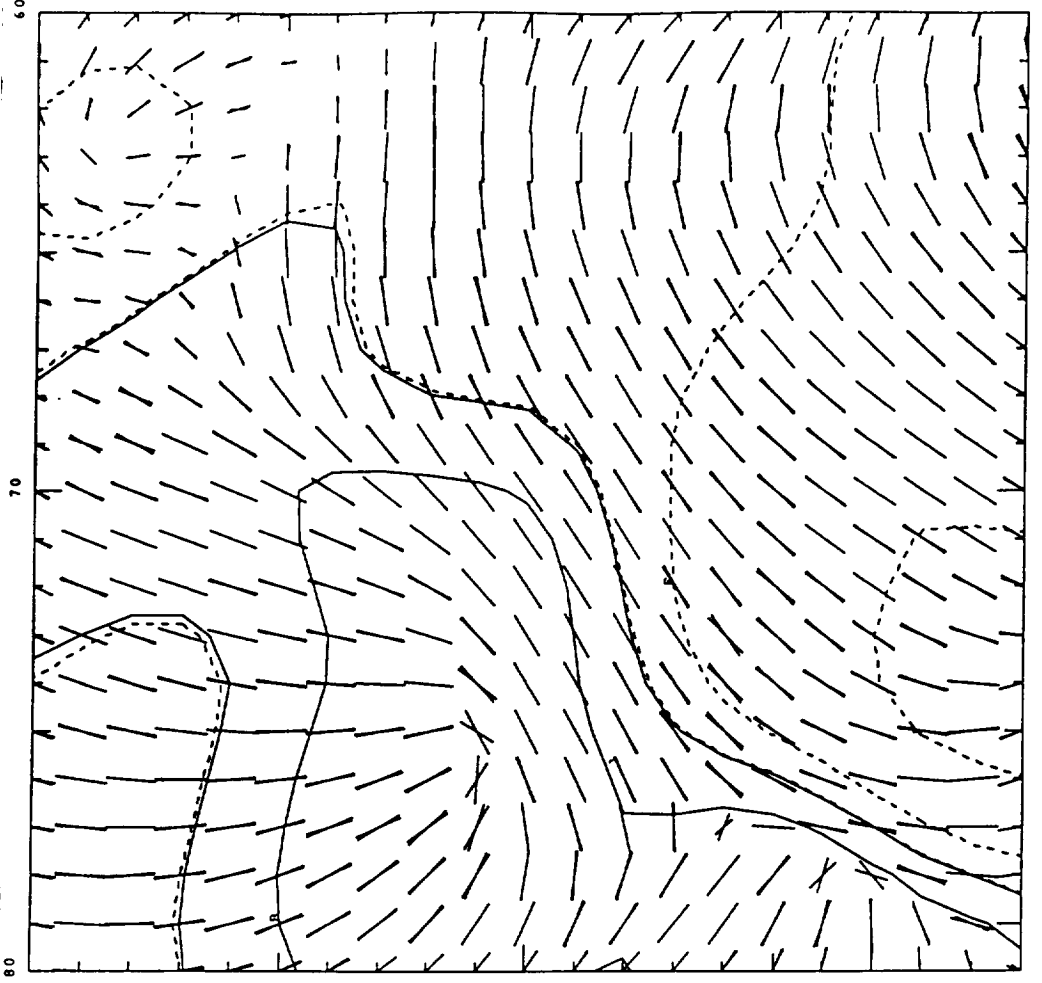
Fig. 3b



(b)



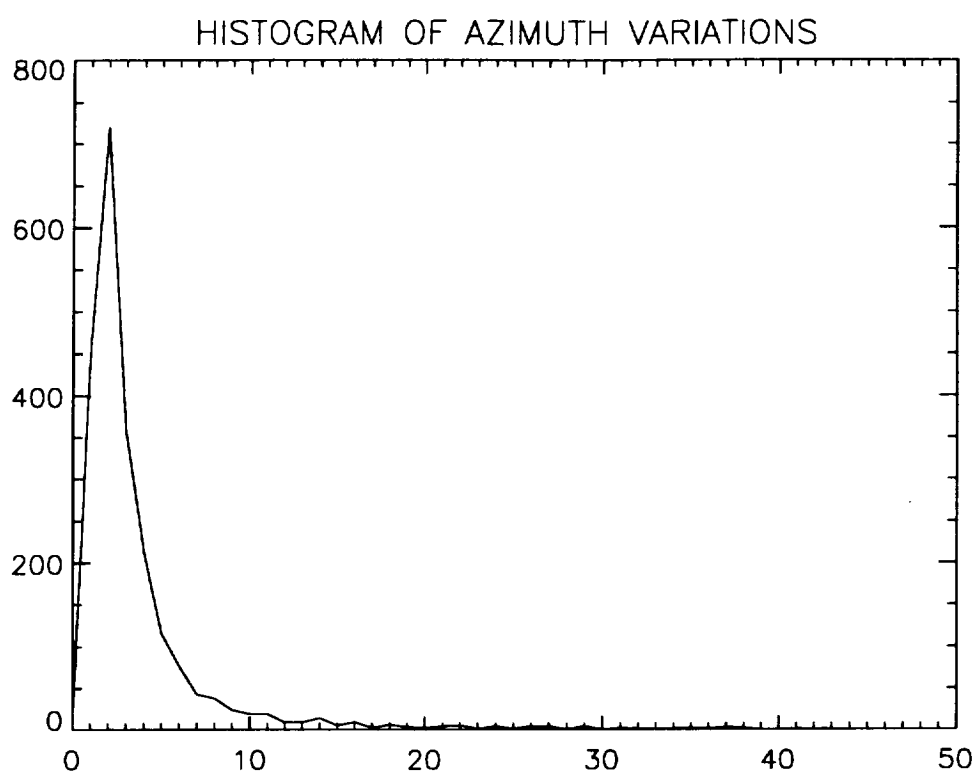
a.



b.

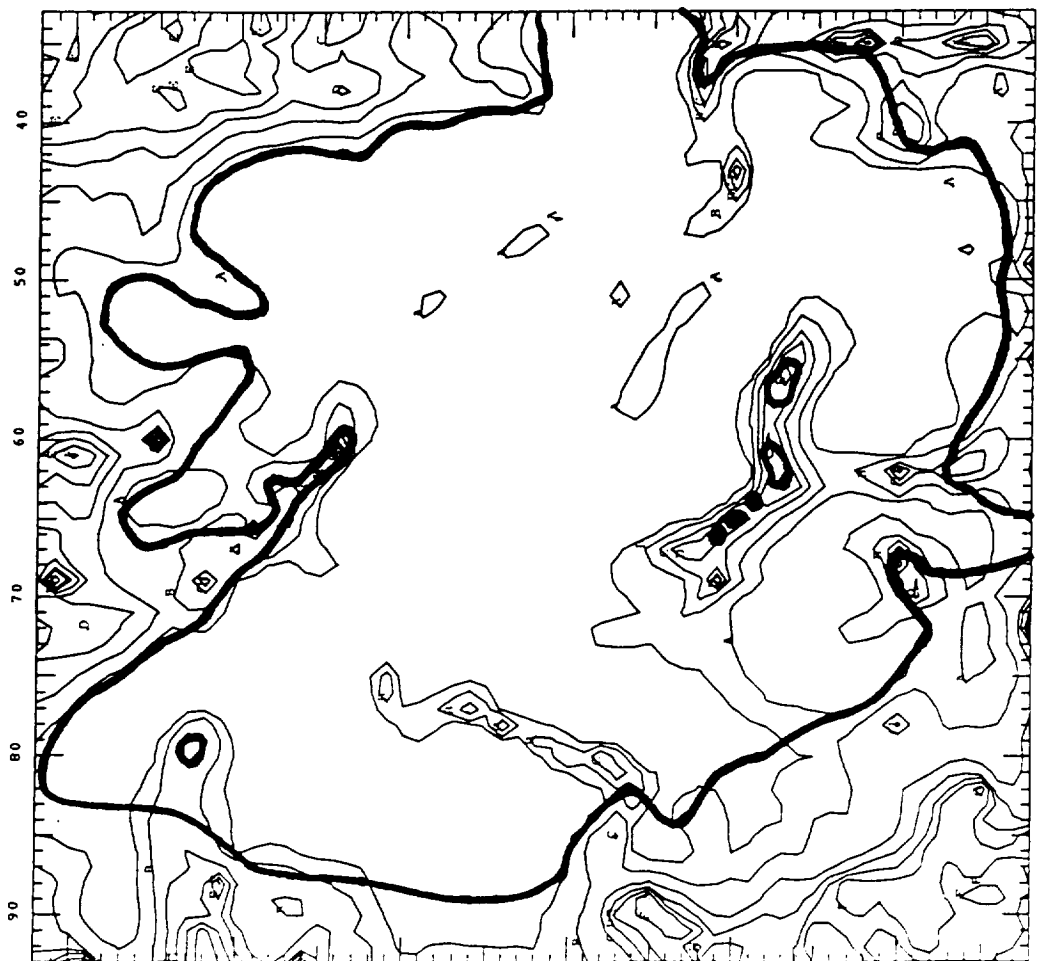
Fig. 4

Fig. 5

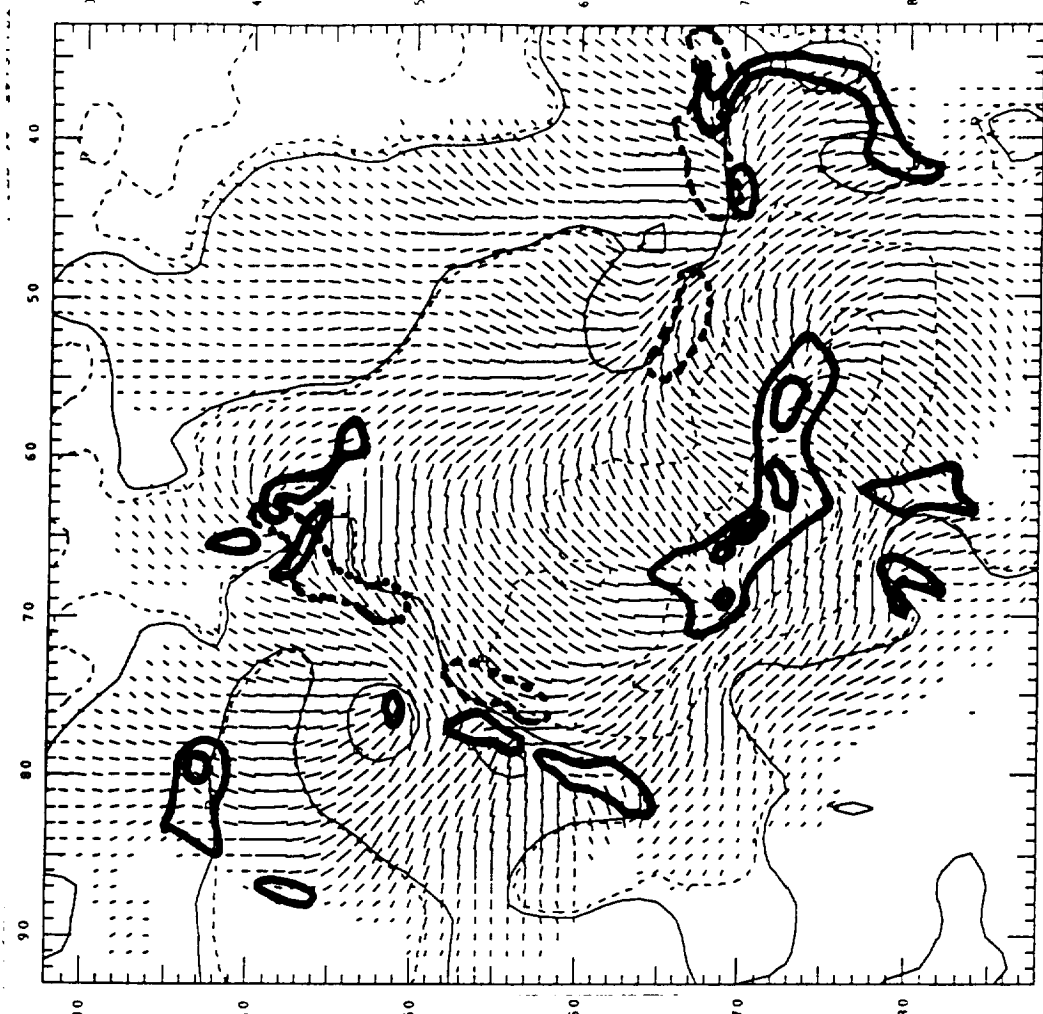


MIN. B = 200.000

BINNING= 1.00000



(a).



(b).

Fig. 6

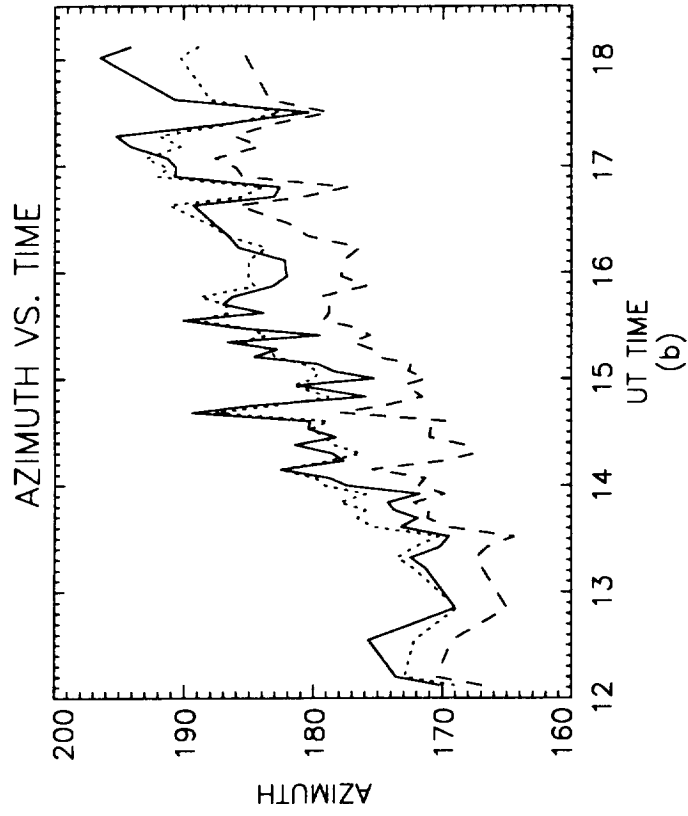
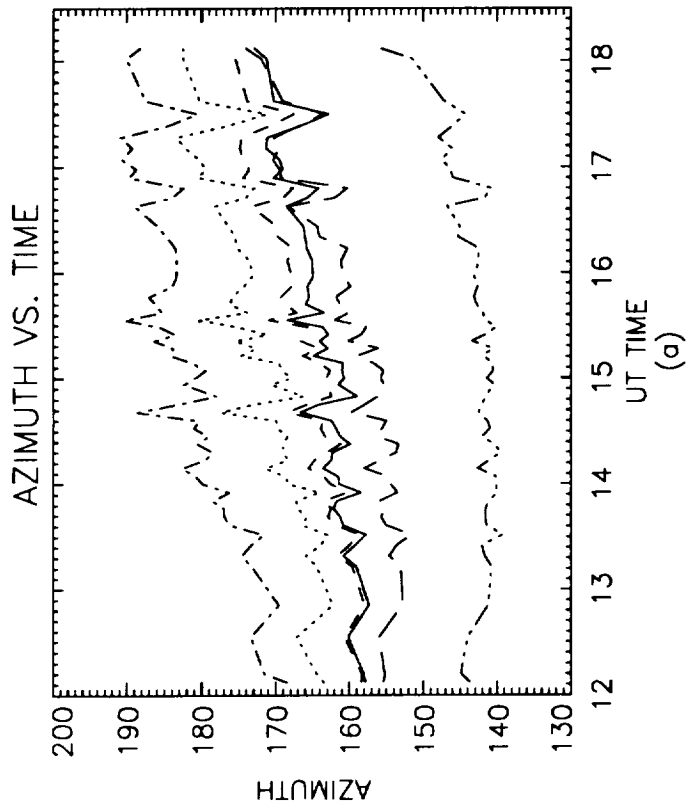


Fig. 7

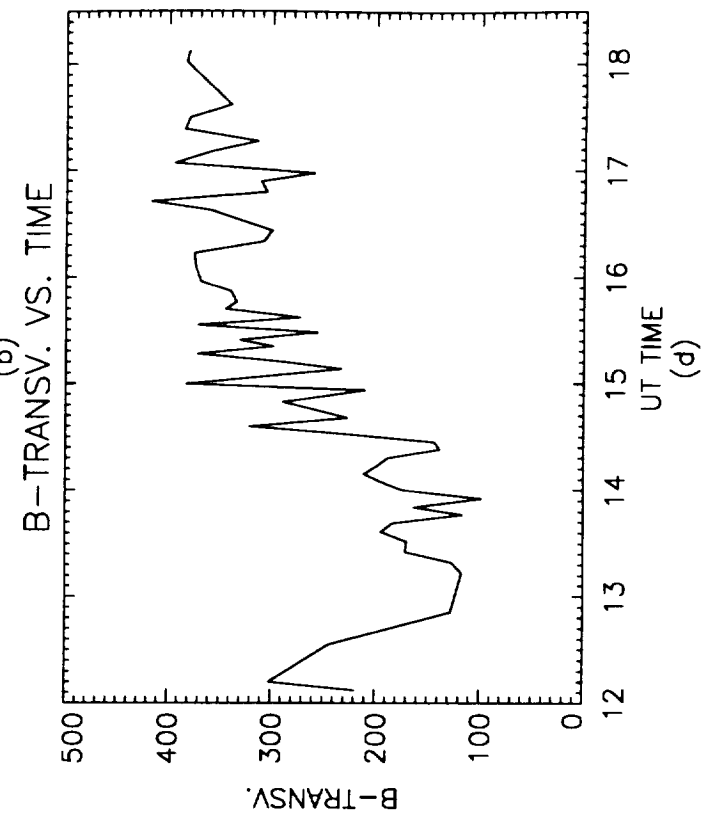
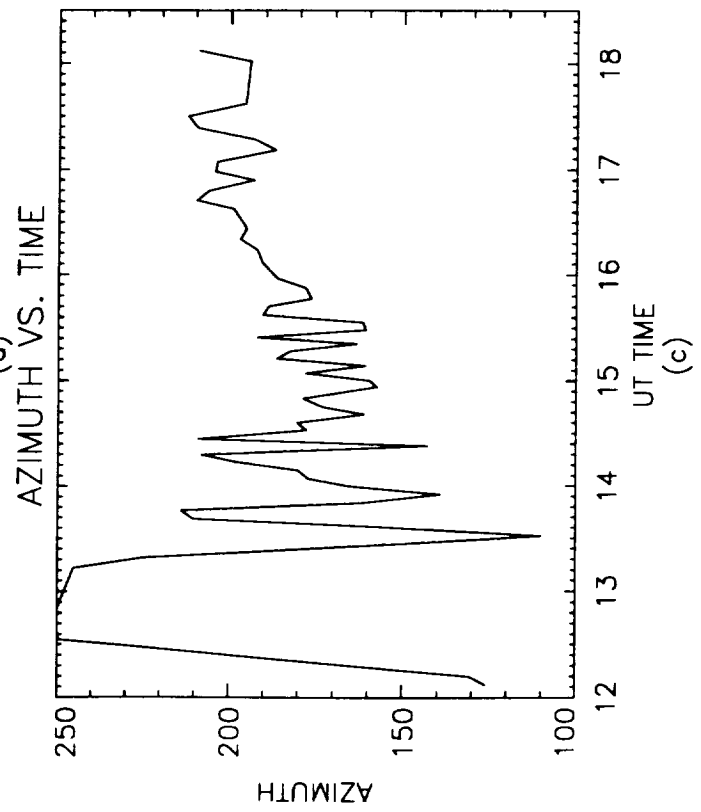
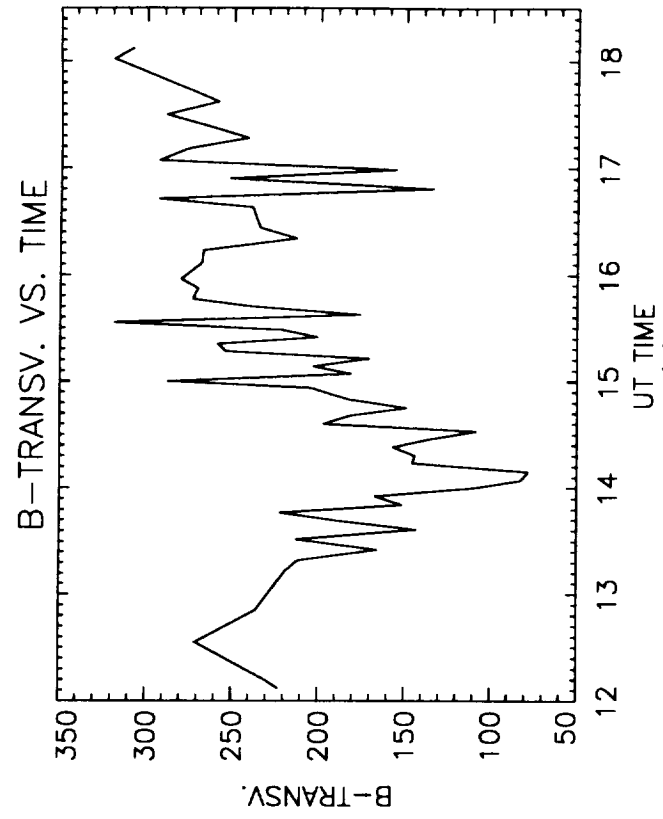
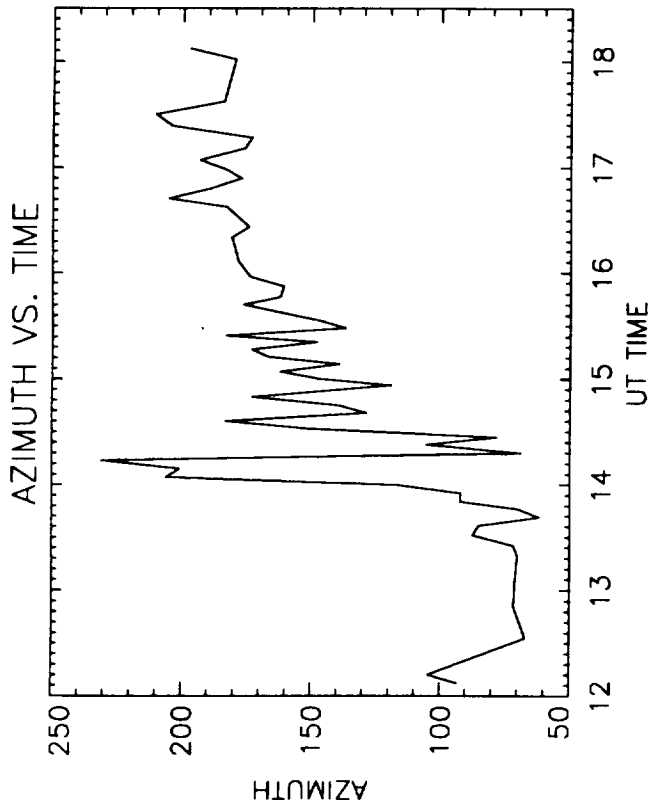
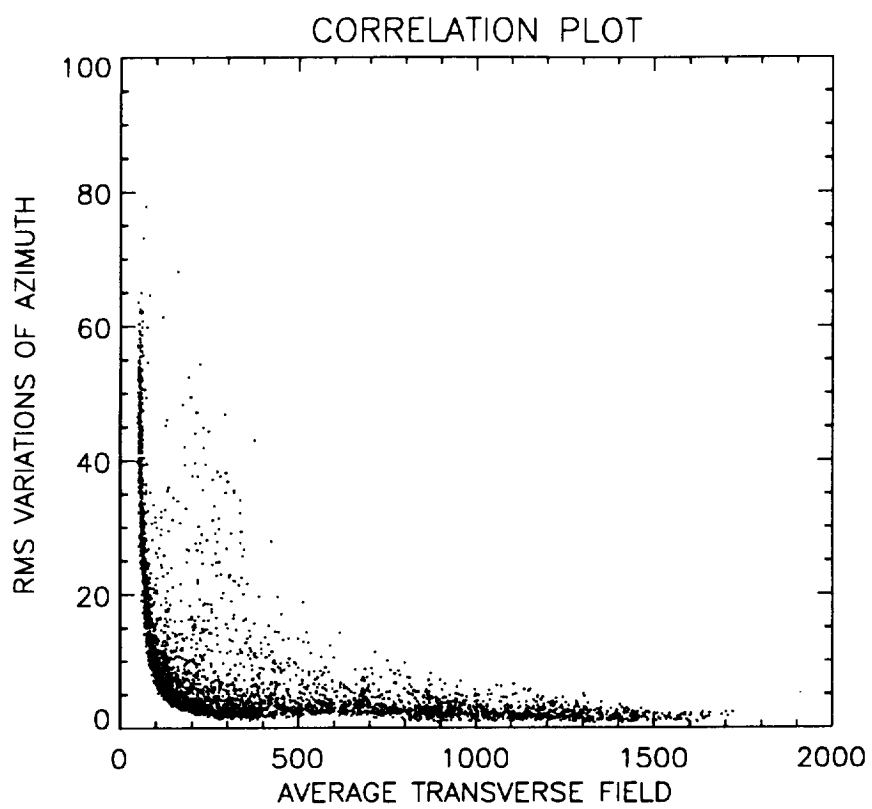


Fig. 8

Fig. 9



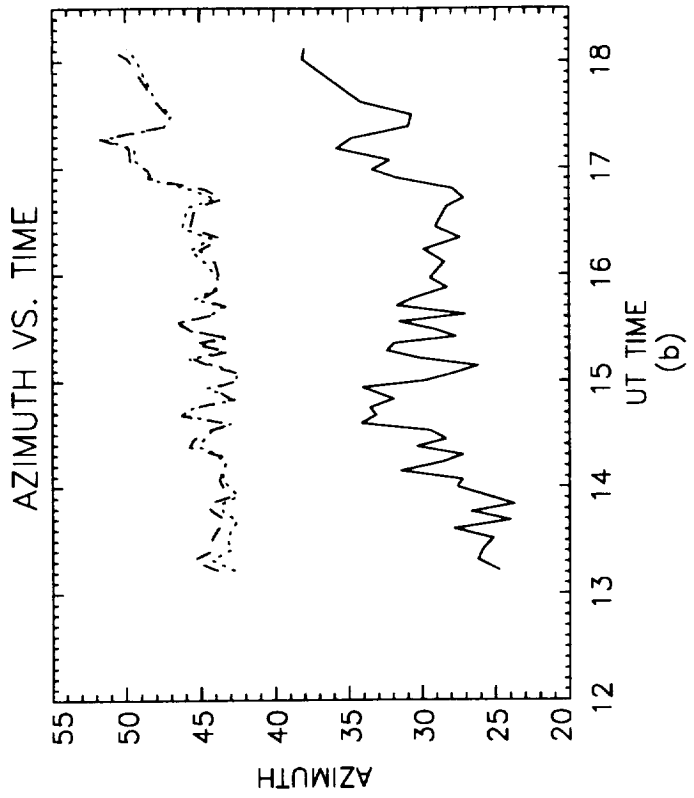
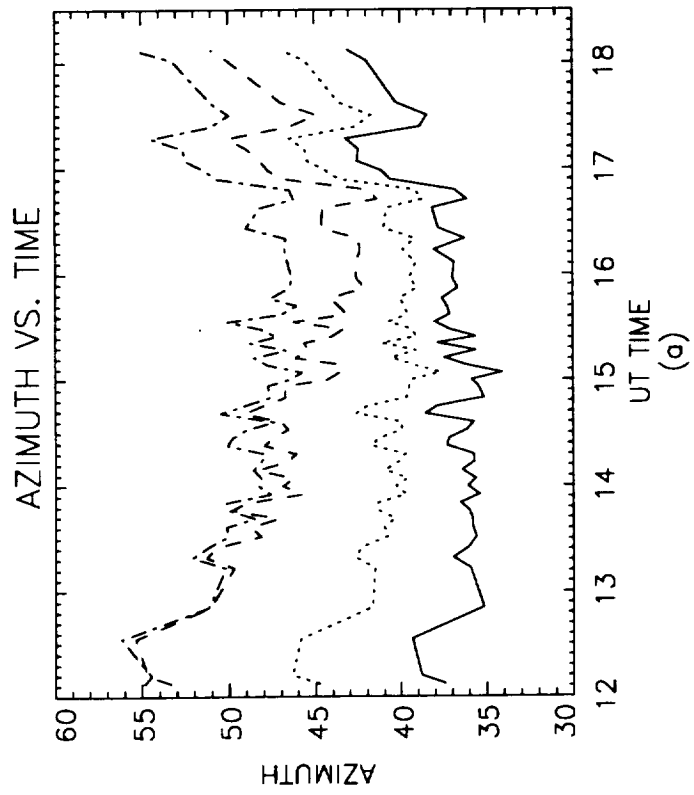


Fig. 10

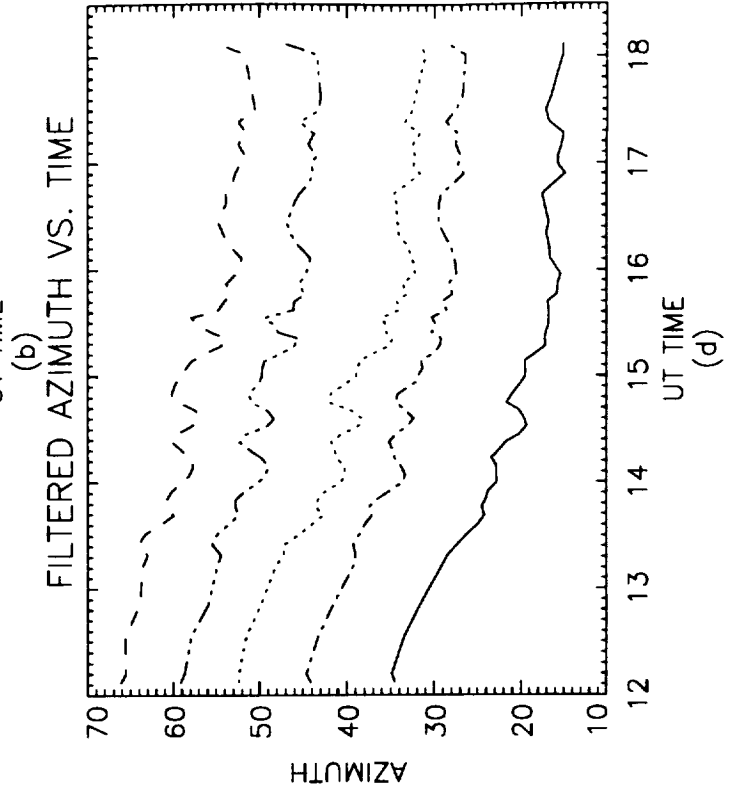
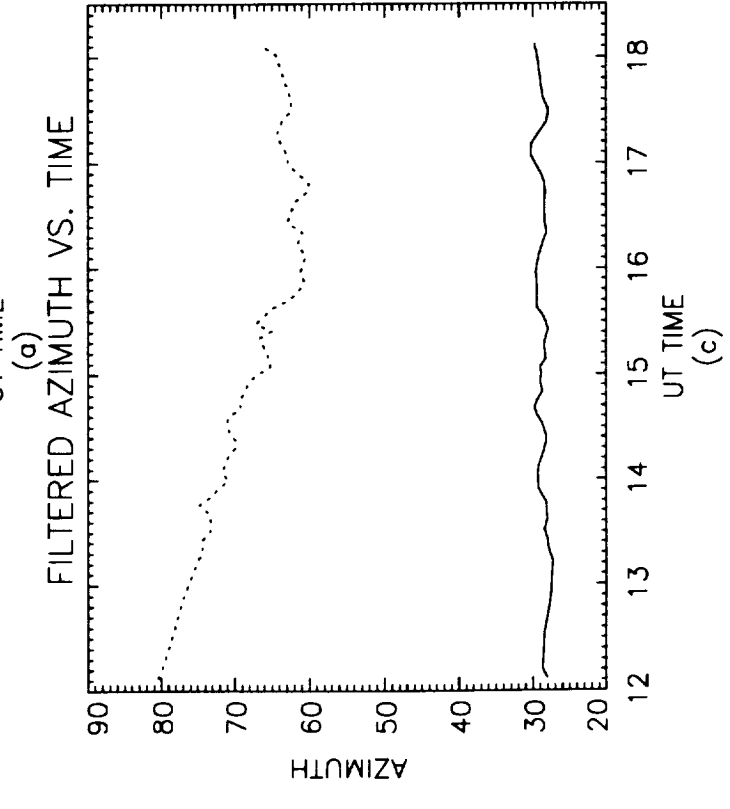
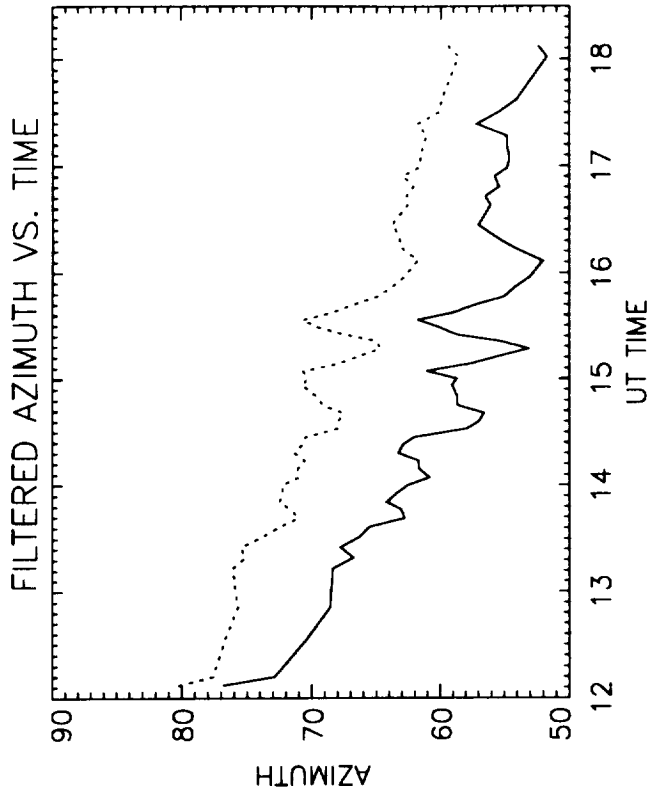
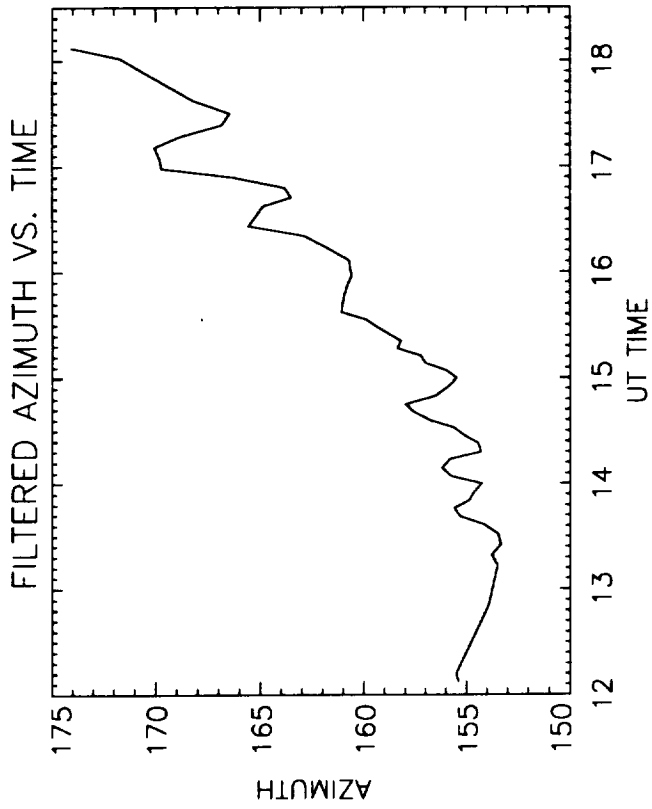


Fig. 11

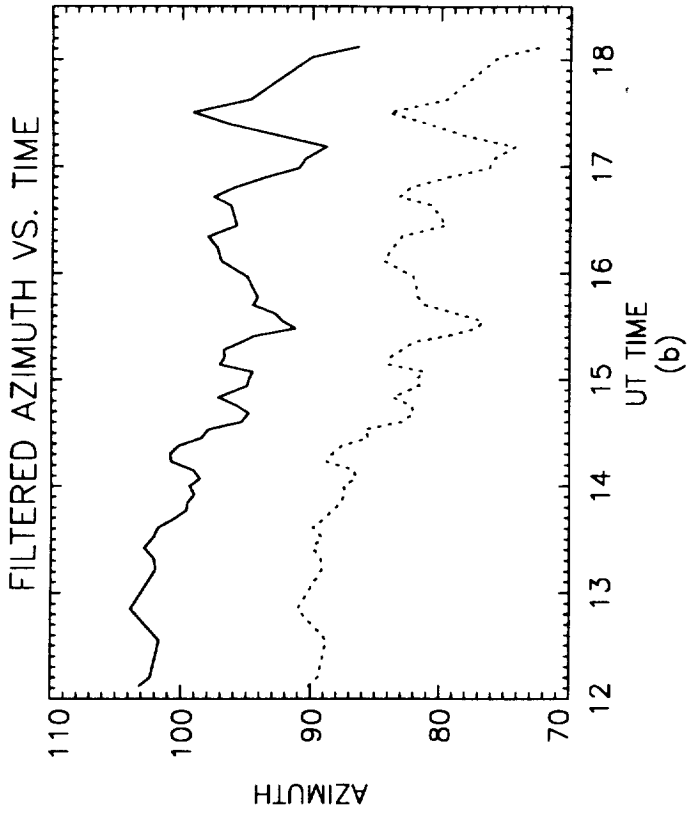
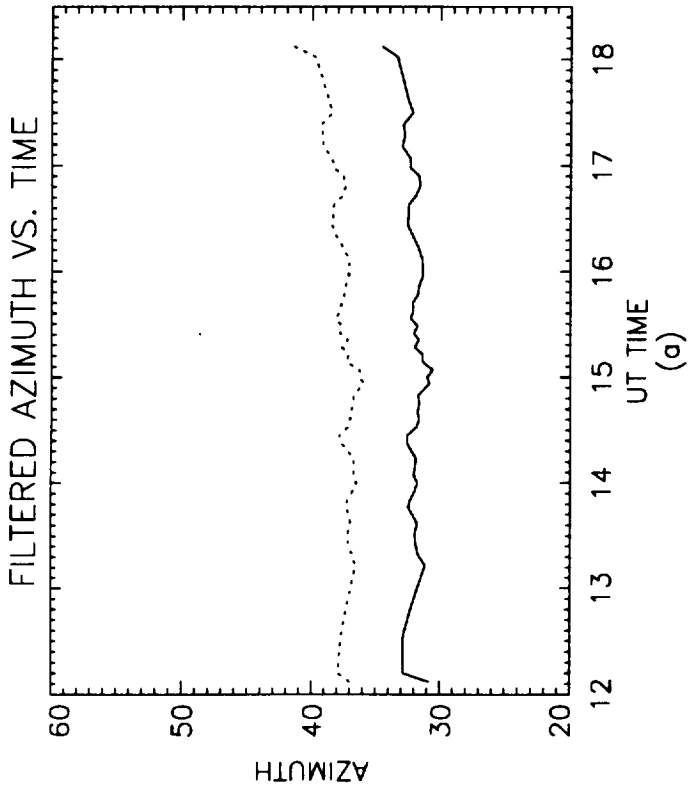


Fig. 12

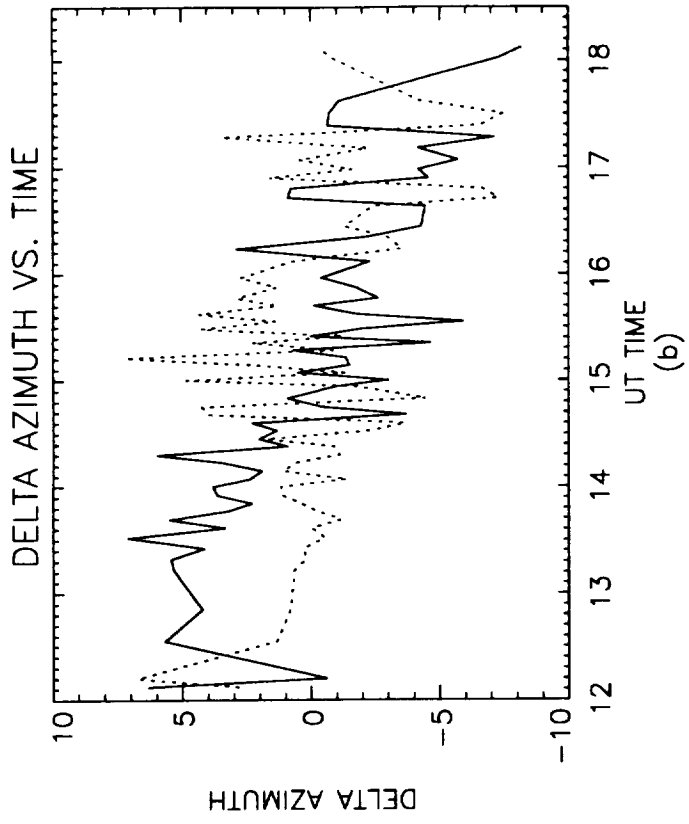
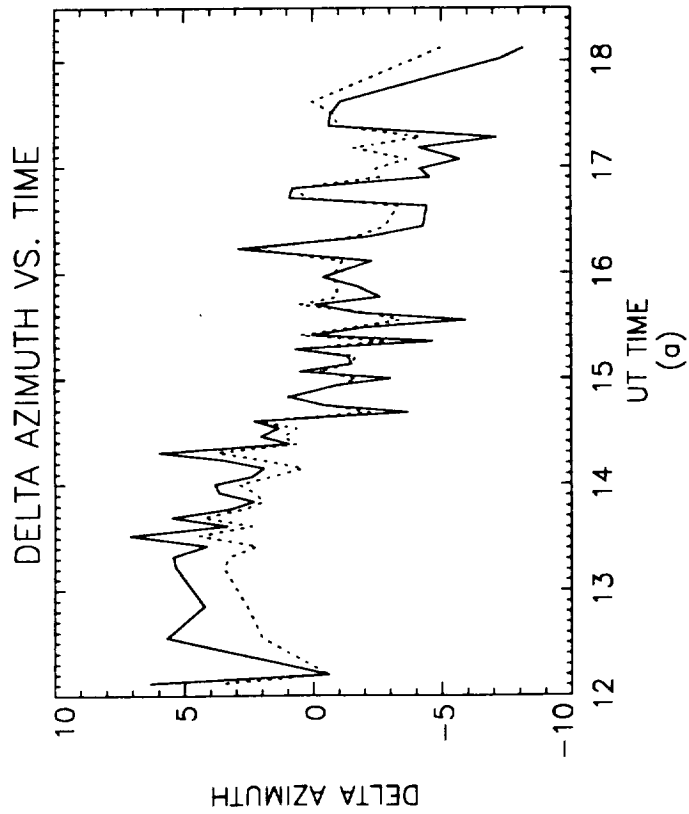


Fig. 13